Hindawi
International Journal of Chemical Engineering
Volume 2018, Article ID 3158147, 11 pages
https://doi.org/10.1155/2018/3158147

Research Article

Carbon Dioxide Absorption Modeling for Off-Gas Treatment in the Nuclear Fuel Cycle

Jorge Gabitto[1] **and Costas Tsouris**[2]

[1]*Department of Chemical Engineering, Prairie View A&M University, Prairie View, TX 77446, USA*
[2]*Oak Ridge National Laboratory, Oak Ridge, TN 37831-6181, USA*

Correspondence should be addressed to Jorge Gabitto; jfgabitto@pvamu.edu

Received 27 February 2018; Revised 2 August 2018; Accepted 8 August 2018; Published 10 October 2018

Academic Editor: Iftekhar A. Karimi

The absorption of carbon dioxide is an important process in many practical applications such as reduction of greenhouse gases, separation and purification processes in the chemical and petroleum industries, and capture of radioactive isotopes in the nuclear fuel cycle The goal of this research is to develop a dynamic model to simulate CO_2 absorption by using different alkanolamines as absorption solvents. The model is based upon transient mass and energy balances for the chemical species commonly present in CO_2 gas-liquid absorption. A computer code has been written to implement the proposed model. Simulation results are discussed. The reported model simulates well the response to dynamic changes in input conditions. The proposed model can be used to optimize and control the separation of carbon-14 in the form of CO_2 in the nuclear industry.

1. Theoretical Considerations

1.1. Introduction. The off-gas stream produced from reprocessing used nuclear fuel containing a host of radioactive gases including tritium, iodine, methyl iodide, krypton, xenon, and carbon dioxide. These gases are hazardous to human health, and some are of considerable economic value. Currently, there is interest in the efficient capture of these gases for recovery or storage purposes [1].

Presently, postcombustion separation of carbon dioxide from flue-gas streams is investigated using membrane separation, low-temperature distillation, physical adsorption by activated carbon and zeolites, chemical absorption by mineral oxides to produce the corresponding carbonates, and chemical absorption by suitable solvents [2]. Chemical absorption by solvents is the most common form of the CO_2 capture process. Amines, and mixtures containing amines, are the most used solvents as these compounds react quickly with CO_2, maintaining high mass transfer-driving forces [2]. Industrially important amines are monoethanolamine (MEA), diethanolamine (DEA), diisopropanolamine (DIPA), and the tertiary amine *N*-methyldiethanolamine (MDEA). Most industrial processes are operated with aqueous amine solutions, but solvents consisting of a mixture of water and a nonaqueous solvent, for example, sulfolane in the Shell-Sulfinol process [3], are also frequently used [4]. Blending of different amines is considered to be attractive because in this way the high absorption capacity of tertiary amines can be combined with the high absorption rates of primary or secondary amines [5]. Blends are also more flexible than singular amines because the relative concentration of the amines can be varied [6]. Other combinations have been considered, such as MEA and 2-amino-2-methyl-1-propanol (AMP). The latter amine is an attractive alternative since it offers higher absorption capacity and lower regeneration energy. Blending MEA with AMP is considered to combine all favorable characteristics of both amines and overcome the unfavorable characteristics [7]. Some studies have been carried out considering the influence of the solvent mixed with the alkanolamines. For example, Usubharatana and Tontiwachwuthikul [8] studied the kinetics of CO_2 capture using methanol mixed into solutions of MEA.

The goal of this work is to develop a theoretical model for dynamic simulations of CO_2 absorption using a generic

blend of amines and/or other solvents. The proposed model can be used to simulate chemical absorption using a wide range of CO_2 input stream concentrations. Through computational implementation, the derived model can be used for design, optimization, and control applications.

1.2. Model Organization. In this work, we will follow an approach similar to the one used by Greer et al. [9] in the dynamic simulation of the absorption/desorption of carbon dioxide from monoethanolamine (MEA). A dynamic model of the absorption process will be developed using a generic mixture of solvents to increase the absorption rate.

Mass transfer rates are calculated using the thin film model with chemical reactions confined to the liquid thin film. Henry's law is used for modeling the vapor-phase equilibrium of CO_2. Henry's constant values for the different gas-phase species are calculated using fugacity ratios obtained by the Peng–Robinson equation of state (EOS). A kinetic scheme is proposed to represent the complex chemical reactions between CO_2 and the solvents. Liquid and vapor energy balances are developed to calculate the liquid and vapor temperature, respectively. A schematic of the column is shown in Figure 1. The model of the absorption tower is developed by taking a small slice of the tower of height *dz*. The height of the packing goes from $z = 0$ to $z = H$, where H is the packing height.

1.3. Kinetic Studies. The most important part of the proposed model is the simulation of the complex chemical reactions involving the solvents and CO_2. In the case of primary and secondary amines, the reaction mechanism is well understood as was originally proposed by Caplow [10] and reintroduced by Danckwerts [11]. CO_2 reacts with the amine through a two-step process. The first step proceeds through the formation of a zwitterion intermediate:

$$\mathrm{RNH_2 + CO_2 \overset{K_1}{\longleftrightarrow} RNH^+COO^-} \tag{1}$$

This step is slow and considered to be the rate-controlling step; it is followed by a very fast removal of a proton by a base:

$$\mathrm{RNH^+COO^- + B_i \overset{K_2}{\longleftrightarrow} RNCOO^- + B_iH^+} \tag{2}$$

It is important to notice that all bases present in the liquid phase will participate in reaction (2); therefore, B_i represents a generic base participating in the reaction with the zwitterion. In this mechanism, the overall forward reaction rate equation can be derived using the quasi-steady-state assumption for the zwitterion intermediate [12]:

$$r_1 = \frac{k_1[\mathrm{CO_2}][\mathrm{RNH_2}]}{1 + (k_{-1}/(\sum_i k_{bi}[B_i]))}, \tag{3}$$

where k_1, k_{-1}, and k_{bi} are the respective specific constants and $\sum_i k_{bi}[B_i]$ represents the summation over the reaction rates of all the bases reacting with the zwitterion present in the solution. In dilute aqueous solutions, for example, the amine, OH^-, and water act as a base, while in nonaqueous solvents, only the amine can be considered a base [12].

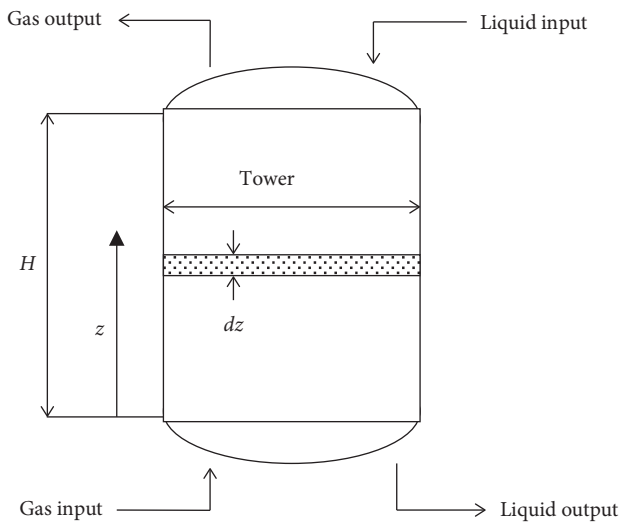

Figure 1: Absorption tower used for carbon dioxide absorption.

In the case of high amine concentration in the solvent, Equation (3) is simplified to

$$r_1 = k_1[\mathrm{CO_2}][\mathrm{RNH_2}]. \tag{4}$$

For aqueous MEA solutions, the overall reaction rate is of second order, and is of first order with respect to the amine. This finding indicates that the deprotonation of the zwitterion by the bases present in the solution is very fast compared to the reverse reaction. Therefore, Equation (4) is considered the main reaction in the absorption of CO_2 in high-concentration aqueous alkanolamine solutions. In the case of low-concentration solutions, more complex rate equations hold [2, 13]. Alvarez-Fuster et al. [14] and Sada et al. [15] showed that changes in the solvent lead also to changes in the order of reaction.

A different mechanism applies to the reaction of CO_2 with ternary amines. According to Littel et al. [16], the reaction of CO_2 with tertiary amines can be described satisfactorily using the base-catalysis reaction mechanism proposed by Donaldson and Nguyen [17]:

$$\mathrm{R_1R_2R_3N + CO_2 + H_2O \overset{K_1}{\longleftrightarrow} R_1R_2R_3NH^+ + HCO_3^-} \tag{5}$$

This mechanism is essentially a base-catalyzed hydration of CO_2; thus, tertiary amines cannot react directly with CO_2. This finding was confirmed by Versteeg and Van Swaaij [18], who studied the absorption of CO_2 into a solution of MDEA and ethanol without water.

In all the cases discussed above, the following CO_2 reactions are also present:

$$\mathrm{CO_2 + H_2O \overset{K_2}{\longleftrightarrow} HCO_3^- + H^+} \tag{6}$$

$$\mathrm{CO_2 + OH^- \overset{K_3}{\longleftrightarrow} HCO_3^-} \tag{7}$$

Reaction (6) is very slow and can be neglected in most circumstances. Reaction (7), however, is fast and can enhance

mass transfer even when the concentration of the hydroxyl ion is low [19].

1.4. Reaction Scheme

1.4.1. Introduction. The components in the gas phase are RNH_2, $R_1R_2R_3N$, CO_2, H_2O, N_2, and O_2, while the species considered in the liquid phase are RNH_3^+, $RNCOO^-$, RNH_2, $R_1R_2R_3N$, $R_1R_2R_3NH^+$, CO_2, H_2O, N_2, O_2, HCO_3^-, OH^-, and H_3O^+. The ionic species remain in the liquid phase, while the others are transferred from one phase to the other according to the scheme shown in Figure 2.

Only gas-phase mass transfer resistance is considered for liquid solvents (H_2O, $R_1R_2R_3N$, and RNH_2), while liquid-only mass transfer resistance for the gas species has been considered: CO_2, N_2, and O_2 ([2], among others). Under certain conditions, however, both resistances have to be considered for the reacting species CO_2. In our computer code, we consider these situations by using a global mass transfer coefficient given by

$$\frac{1}{K^{l}_{CO_2}} = \frac{1}{Ek^{l}_{CO_2}} + \frac{H^{cc}}{k^{g}_{CO_2}}. \tag{8}$$

where $K^{l}_{CO_2}$ is the overall mass transfer coefficient based upon liquid-phase concentrations; $k^{l}_{CO_2}$ is the liquid-phase mass transfer coefficient; $k^{g}_{CO_2}$ is the gas-phase mass transfer coefficient; $H^{cc} = C^{l}_i/C^{g}_i$ is the concentration-based Henry's constant, in which C^{l}_i and C^{g}_i are the liquid- and gas-phase i-species concentrations, respectively; and E is the enhancement factor defined in the subsection below. Typical values of these coefficients are given in Table 1. In Table 2, all the chemical species considered in the model are included.

1.4.2. Reactions. Mandal et al. [20] and Benamor and Aroua [21] proposed the following set of reactions occurring in the aqueous primary amine solution. A gas-liquid equilibrium equation and six chemical equilibria equations are introduced to describe the chemistry involved in CO_2 absorption:

$$2RNH_2 + CO_2 \overset{K_1}{\longleftrightarrow} RNHCOO^- + RNH_3^+ \tag{9}$$

$$CO_2 + H_2O \overset{K_2}{\longleftrightarrow} HCO_3^- + H^+ \tag{10}$$

$$CO_2 + OH^- \overset{K_3}{\longleftrightarrow} HCO_3^- \tag{11}$$

$$H_2O \overset{K_4}{\longleftrightarrow} OH^- + H^+ \tag{12}$$

$$RNH_3^+ \overset{K_5}{\longleftrightarrow} RNH_2 + H^+ \tag{13}$$

$$RNHCOO^- + H_2O \overset{K_6}{\longleftrightarrow} RNH_2 + HCO_3^- \tag{14}$$

$$CO_2\,(\text{gas}) \longleftrightarrow CO_2\,(\text{liquid}) \tag{15}$$

Following Bosch et al. [6] who studied blends of alkanol amines, we add reaction (5) catalyzed by ternary amines and reaction (16) to account for the decomposition of the ternary ammonium ion:

$$R_1R_2R_3NH^+ \overset{K_{15}}{\longleftrightarrow} R_1R_2R_3N + H^+ \tag{16}$$

Reactions (5), (9), and (11) are the main reactions in CO_2 absorption by amines. The other reactions are required to complete the total reaction mechanism [6]. The CO_2 loading rate, defined as the ratio of CO_2 to alkanolamines, determines the relative weight of all reactions. For CO_2 loading rates below 0.5, Equation (9) is the main reaction. In the case of loading rates above 0.5, reaction (11) predominates, while reaction (5) will be important only for large amounts of ternary amine in the feed. In this work, we are interested in small loading rates and significant amounts of ternary amine present; therefore, the reactions with the amines will be the most important ones. A list of all

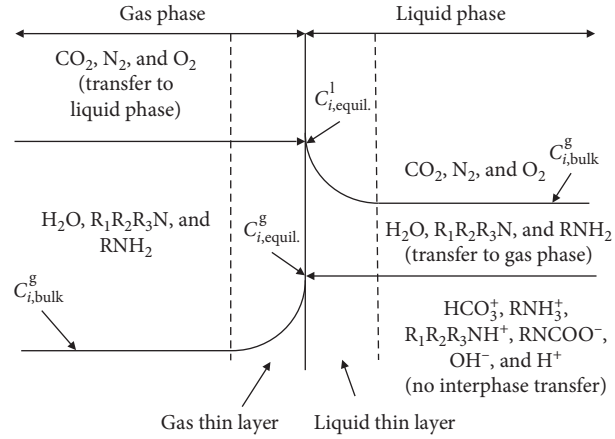

Figure 2: Concentration gradients at the vapor-liquid interphase.

Table 1: List of chemical species participating in the reaction scheme.

Compound number	Gas	Liquid
1	N_2 (g)	$RNHCOO^-$
2	O_2 (g)	RNH_3^+
3	CO_2 (g)	HCO_3^-
4	H_2O (g)	OH^-
5	RNH_2 (g)	RNH_2 (l)
6	$R_1R_2R_3N$ (g)	CO_2 (l)
7	—	H^+ (l)
8	—	$R_1R_2R_3N$ (l)
9	—	$R_1R_2R_3NH^+$ (l)

Table 2: Typical values for CO_2 mass transfer calculations.

Property	Unit	Value
H^{cc}	M_{liquid}/M_{gas}	1.23
E	Dimensionless	67.9
$k^{g}_{CO_2}$	m/s	0.0594
$k^{l}_{CO_2}$	m/s	$8.65\ 10^{-5}$
$k^{l}_{CO_2}E$	m/s	0.00587
$K^{l}_{CO_2}$	m/s	0.00524
Relative error	Dimensionless	10.7%

reactions used in the model is included in Appendix. Equation (15) is considered by using the corresponding Henry's law constant for CO_2.

1.4.3. Kinetic Parameters. Kinetic data were collected using a general primary-secondary amine that follows the zwitterion mechanism represented by Caplow [10] and Danckwerts [11]. The forward reaction (9) is thought to occur through a two-step mechanism. Initially, a CO_2 molecule and an alkanolamine molecule form a zwitterion intermediate which, in a second step, reacts with another alkanolamine molecule. The second step is much faster than the first step; hence, the first step is rate limiting and of second order. The reaction rate is given by

$$-r_1 = k_{1f}[CO_2][RNH_2]\left(\text{mol}\cdot\text{s}^{-1}\cdot\text{m}^{-3}\right). \quad (17)$$

The specific forward rate constant k_{1f} is calculated using the method in [22]:

$$k_{1f} = \exp\left[\frac{24.4 - 6864}{T_1}\right]\left(\text{m}^3\cdot\text{mol}^{-1}\cdot\text{s}\right). \quad (18)$$

The bicarbonate ion formation, reaction (11), is the most important reaction for CO_2/alkanolamine loadings above 0.5. It is of second order, given by

$$-r_3 = k_{3f}[CO_2][OH^-]\left(\text{mol}\cdot\text{s}^{-1}\cdot\text{m}^{-3}\right). \quad (19)$$

The forward rate for the formation of bicarbonate is significantly fast, but the overall rate is usually quite small due to the low concentration of OH^- ions used. At loadings of CO_2/alkanolamines above 0.5, this becomes the dominant reaction for CO_2 removal. The forward rate is calculated from [23]:

$$k_{3f} = \exp\frac{\left[31.396 - 6658.0/T_1\right]}{1000}\left(\text{m}^3\cdot\text{mol}^{-1}\cdot\text{s}^{-1}\right). \quad (20)$$

In order to complete the rate calculations, we collected literature data corresponding to the equilibrium rate constants of reactions (9)–(14) from Bedelbayiev et al. [24] and Greer [2]. In order to deal with reactions (5) and (16) for ternary alkanol amines, we followed many investigators including Haimour et al. [25], Critchfield [26], Littel et al. [16], and Rangwala et al. [27] who fit the rate constant of the reaction as a function of temperature using

$$k_i = k_i^{\text{o}} \exp\left[-\frac{E_a}{RT}\right]. \quad (21)$$

All values of kinetic parameters used are listed in Table 3. A full description of all the rate equations and calculation of generation terms is also included in Appendix.

1.4.4. Enhancement Factor. The carbon dioxide absorption is accompanied by strong chemical reactions. Therefore, the calculation of the CO_2 flux term requires the use of an enhancement factor (E) to account for the enhanced mass transfer. The enhancement factor is defined as the mass transfer rate under reactive absorption divided by the mass transfer rate under nonreactive absorption conditions [31]. The CO_2 molar flow term ($N_{CO_2,\text{diff}}$) is given as follows [2, 9, 24]:

$$N_{CO_2,\text{diff}} = -k^{\text{l}}_{CO_2} E a_{\text{w}} H^{\text{cc}} C^{\text{g}}_{CO_2}, \quad (22)$$

where a_{w} is the interphase area per unit volume. The enhancement factor (E) is a function of the Hatta number (Ha) defined as

$$\text{Ha} = \frac{\sqrt{D_{CO_2}\left(k_{1f}C_{RNH_2} + k_{3f}C_{OH^-} + k_{5f}C_{R_1R_2R_3N}\right)}}{k_l}, \quad (23)$$

where D_{CO_2} is the diffusion coefficient and k_{if} are the forward specific reaction rate constants. The influence of the different reactions on the total rate of CO_2 absorption is considered by the enhancement factor E. The Hatta number is the ratio of the rate of homogeneous reaction relative to the rate of gas dissolution. Ha is also a measure of the amount of dissolved gas that reacts inside the diffusion film near the gas-liquid interface compared to the amount that reaches the bulk of the solution without reacting. When Ha = 0, we have purely physical absorption. The higher the value of the Hatta number, the stronger the effect of chemical reactions on mass transfer. In the case of Ha > 2, the enhancement factor E is directly equal to Ha [31].

Versteeg et al. [32] recommended a different definition of the Hatta number including C_{CO_2} instead of C_{NaOH} in Equation (23) to calculate the enhancement factor when all RNH_2 is consumed, and reaction (3) is the dominant CO_2 removal reaction. Other authors have used *both* formulations with similar results [24, 33, 34]. In this work, however, we preferred to use the general definition of the Hatta number, Equation (23).

1.5. Mass Transfer Model

1.5.1. Mass Balances. The mass balance of component i in the liquid phase was calculated using the following equation [2, 35]

$$\frac{\partial C^{\text{l}}_i}{\partial t} = u_l \frac{\partial C^{\text{l}}_i}{\partial z} - N_{i,\text{diff}} + R_{\text{gen},i}, \quad (24)$$

where u_{l} is the superficial liquid-phase velocity, $R_{\text{gen},i}$ represents moles of species i generated/consumed by interphase reaction per unit volume, and $N_{i,\text{diff}}$ is the mass flow of component i from the liquid phase into the gas phase. In the model presented in this work, the effect of reaction on the CO_2 absorption is considered through the use of the enhancement factor. In the cases of ionic species, there is no interphase mass transfer; therefore, for these reactions, Equation (24) becomes

$$\frac{\partial C^{\text{l}}_i}{\partial t} = u_{\text{l}} \frac{\partial C^{\text{l}}_i}{\partial z} + R_{\text{gen},i}. \quad (25)$$

The generic amines (RNH_2 and $R_1R_2R_3N$) are the only chemical species for which we have to calculate a generation term plus an interfacial mass transfer term ($N_{RNH_2,\text{diff}}$ and $N_{R_1R_2R_3,\text{diff}}$).

Table 3: Information used in solving the proposed reaction model.

Equation no. (reaction)	Forward rate (k_{fi})	Equilibrium constant	Reverse rate (k_{ri})
(B.1) (9)	$k_{1f} = \exp(24.4 - 6864/T_l)$ (Reference [22])	$K_1 = K_2/(K_5 * K_6)$ (Reference [2])	$k_{1r} = (k_{1f})/K_1$
(B.2) (10)	$k_{f2} = 0.024$ (Reference [28])	$K_2 = 1E6 * \exp(231.465 - 12092.1/T_l - 36.782 * \ln(T_l))$ (Reference [29])	$k_{2r} = (k_{2f})/K_2$
(B.3) (11)	$k_{3f} = \exp[31.396 - 6658/T_l] * 1E{-}3$ (Reference [23])	$K_3 = \exp(31.396 - 6658/T_l)/1000$ (Reference [2])	$k_{3r} = (k_{3f})/K_3$
(B.4) (12)	$k_{4f} = 2E - 5$ (Reference [30])	$K_4 = 9.234E19 * \exp(0.0772 * T_l)$ (Reference [29])	$k_{4r} = (k_{4f})/K_4$
(B.5) (13)	$k_{5f} = 0.1$ (Reference [2])	$K_5 = 1E6 * \exp(0.8{-}8094.8/T_l - 0.00748 * T_l)$ (Reference [29])	$k_{5r} = (k_{5f})/K_5$
(B.6) (14)	$k_{6f} = 0.1$ (Reference [2])	$K_6 = 2E5 * \exp(1.283 - 3456.2/T_l)$ (Reference [29])	$k_{6r} = (k_{6f})/K_6$
(B.7) (5)	$k_{7f} = 2.5E - 3\ \exp(23.17 - 6894.8/T_l)$ (Reference [12])	$K_7 = K_2/K_9$ (Reference [12])	$k_{7r} = (k_{7f})/K_7$
(B.8) (16)	$K_{8f} = 0.1$ (Reference [19])	$K_8 = 1E6 * \exp(0.8 - 8094.8/T_l - 0.00748 * T_l)$ (Reference [29])	$k_{8r} = (k_{8f})/K_8$

1.6. Energy Balances. The reactions given by Equations (8) and (11) are highly exothermic; therefore, an energy balance has to be solved in order to consider temperature changes. The heat of reactions for Equations (9) and (11) used was 65 kJ/molCO_2 and 20 kJ/molCO_2, respectively. The first value was taken from Greer [2] and the second from Pinsent et al. [28].

A two-equation model for the transient energy balance in the control volume depicted in Figure 1 leads to the following equations for all the components shown in the figure [9, 36]:

$$\frac{\partial T^{l}}{\partial t} = -u_l \frac{\partial T^{l}}{\partial t} - N_{CO_2,diff} \frac{\Delta H_R}{\sum_i C_i^{l} C_{pi}^{l}} - U_T a_w \frac{(T^{l} - T^{g})}{\sum_i C_i^{l} C_{pi}^{l}}, \quad (26)$$

$$\frac{\partial T^{g}}{\partial t} = -u_g \frac{\partial T^{g}}{\partial t} - U_T a_w \frac{(T^{l} - T^{g})}{\sum_i C_i^{g} C_{pi}^{g}}, \quad (27)$$

where C_{pi}^{g} and C_{pi}^{l} are the heat capacities of component i in the mixture, U_T is the global heat transfer coefficient, u_g is the superficial velocity inside the gas phase, and ΔH_R is the heat released by the chemical reaction. The CO_2 molar flow term ($N_{CO_2,diff}$) is given by Equation (22), while the enhancement factor (E) is given by the Hatta number defined by Equation (23).

1.7. Thermodynamics. The molar flow of component i from the gas phase into the liquid phase ($N_{i,diff}^{g}$) is calculated using

$$N_{i,diff}^{g} = -k_i^{l} a_w \left(C_i^{l} - C_i^{*}\right), \quad (28)$$

where C_i^{*} is the interfacial liquid equilibrium concentration. In order to evaluate C_i^{*}, we use a formulation based upon the calculation of gas and liquid fugacity values [2]. This formulation avoids the use of an iterative procedure as the fugacity values can be calculated directly as

$$N_{i,diff}^{g} = \frac{k_i^{g} a_w}{\varphi_i^{g} Z^{g} R T^{g}} \left(f_i^{l} - f_i^{g}\right). \quad (29)$$

This expression for the diffusion molar flow is valid for the RNH_2, $R_1R_2R_3N$, and H_2O components when the resistance is assumed to be in the gas-liquid film [2]. A similar expression for CO_2, O_2, and N_2 can also be derived by

$$N_{i,diff}^{l} = \frac{-k_i^{l} a_w}{\varphi_i^{l} P} C_T^{l} \left(f_i^{g} - f_i^{l}\right). \quad (30)$$

In Equations (29) and (30), R is the ideal gas constant; P is the pressure; T is the temperature; C_T^{l} is the total molar concentration in the liquid phase; Z_g is the gas-phase compressibility factor; f_i^{l} and f_i^{g}, are the fugacities of component i in liquid and gas phases, respectively; and φ_i^{l} and φ_i^{g}, are the fugacity coefficients for component i in the liquid and gas phases, respectively.

2. Results and Discussion

2.1. Model Validation. A FORTRAN computer code was developed based upon a previous one prepared for simulating CO_2 absorption using primary/binary amine solvents [30]. An explicit finite-difference scheme was used to solve the relevant hyperbolic partial differential equations. For convenience, in our equations, all variables were made dimensionless, but the species concentrations were calculated in dimensional values (mM and mol/m^3). The residence time of the liquid phase ($t_r = H/u_l$) was used to define a dimensionless time (t = time/t_r). In all our simulation runs, we used geometric parameters and operating conditions taken from the literature. A list of our input data is shown in Table 4. This list includes information about the packing, the ranges of all values, and the standard set used in most of our calculations.

Validation of the computer code was achieved by comparing calculated parameters with data from the literature, especially with the work of Greer [2]. The validation process included checking against literature values [2, 5, 6, 23, 26, 39] the values of our calculated geometric parameters (d_p, a_T, and a_w), transfer coefficients (k_i^{l} and k_i^{g}), kinetic parameters (k_{if}, k_{ir}, K_i, and E), and equilibrium parameters (H^{cc}, f_i^{g}, f_i^{l}, φ_i^{g}, and ϕ_i^{l}). It also included a comparison of calculated mass species concentration profiles against literature values [2, 5, 23, 26, 30].

In Figure 3, we show a comparison of calculated CO_2 axial concentration profiles against those values reported by Greer [2] for dimensionless time (t) equal to 0.328 (2000 s) and steady-state condition. The basic set of parameters and operating conditions reported by Greer ([2] Table 4.2 in page 90) was used in these calculations. It can be seen in the

Table 4: Typical values of column geometric parameters and operating variables.

Parameter	Unit	Default value	Range	Reference
Height	M	5	1–10	Richardson et al. [37]
Tower diameter	M	1	0.5–2	Richardson et al. [37]
Dry specific area (a_T)	m^2/m^3	200	200–500	Billet and Schultes [38]
Void fraction (ε)	m^3/m^3	0.979	0.979	Billet and Schultes [38]
Packing equivalent diameter	M	0.01	0.005–0.02	Billet and Schultes [38]
Packing coefficient (C_l)	Dimensionless	0.971	0.971	Billet and Schultes [38]
Packing coefficient (C_h)	Dimensionless	0.547	0.547	Billet and Schultes [38]
Packing coefficient (C_v)	Dimensionless	0.390	0.390	Billet and Schultes [38]
Liquid-phase superficial velocity (u_l)	m/s	0.01	0.001–0.1	Greer [2]
Gas-phase superficial velocity (u_g)	m/s	1	0.5–5	Greer [2]
Input temperature	K	313	293–323	Greer [2]
CO_2 concentration	mol/m^3	1.7	0.017–17.0	This work
RNH_2 molar fraction	Dimensionless	0.2	0.01–0.5	Greer [2]
$R_1R_2R_3N$ molar fraction	Dimensionless	0.1	0.01–0.2	This work

figure that there is good agreement between our calculated data and those from Greer [2] for the CO_2 axial concentration profiles; our calculated values, however, were always slightly lower than those reported by Greer [2]. Similar agreement, not shown in this work, was achieved when calculating the other chemical compounds' axial profiles.

The accuracy of the reaction model was validated by carrying out a mass balance for the amine chemical species. A global mass balance for the amines and their reaction products at equilibrium gives

$$u_l A_{sec.} [RNH_2]_{IN} = u_l A_{sec.} \left([RNH_2]_{IOUT} + [RNH_3^+]_{OUT} + [RNHCOO^-]_{OUT} \right), \quad (31)$$

$$u_l A_{sec.} [R_1R_2R_3N]_{IN} = u_l A_{sec.} \left([R_1R_2R_3N]_{IOUT} + [R_1R_2R_3N^+]_{OUT} \right). \quad (32)$$

The difference between both sides in Equations (31) and (32) was used as a way of estimating the accuracy of the reaction scheme. In all our calculations, the error between the calculated concentrations was on the order of the code precision (10^{-6}). A global mass balance for CO_2 was used as another way of estimating the global accuracy of the proposed model. The biggest relative error in all our calculations was 0.01%.

2.2. Simulation Results. The time change of the CO_2 concentration is depicted in Figure 4, where typical axial concentration profiles are presented. At dimensionless time equal to 0, a gas mixture containing CO_2 is injected. The CO_2 concentration is highest at the base of the column, $Z = 0$, and drops as we approach the top, $Z = 1$. The results in Figure 4 show that as time increases, the concentration of CO_2 increases as we approach the top. We can also see that, at long times, the steady state is achieved.

In order to study the time evolution of the concentration of the generic amine, we chose to use monoethanolamine (MEA) due to the high amount of data available for this particular chemical compound. MEA reacts with CO_2 following reaction (9). Two amine ions, the ammonium-like ion

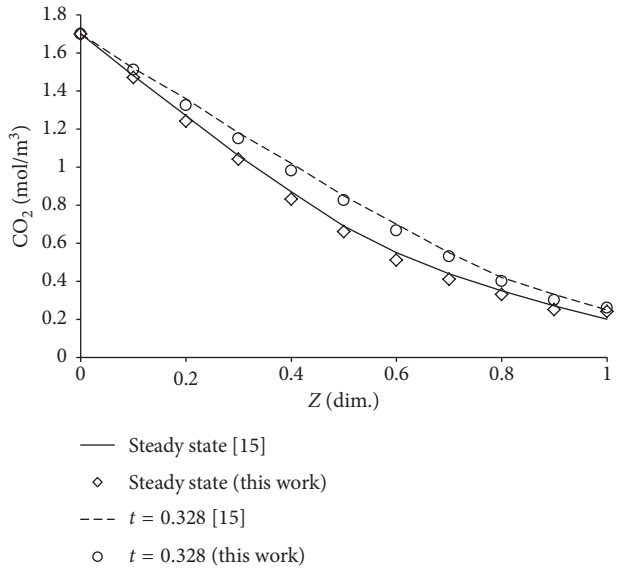

Figure 3: Comparison of carbon dioxide axial concentration profiles with literature data.

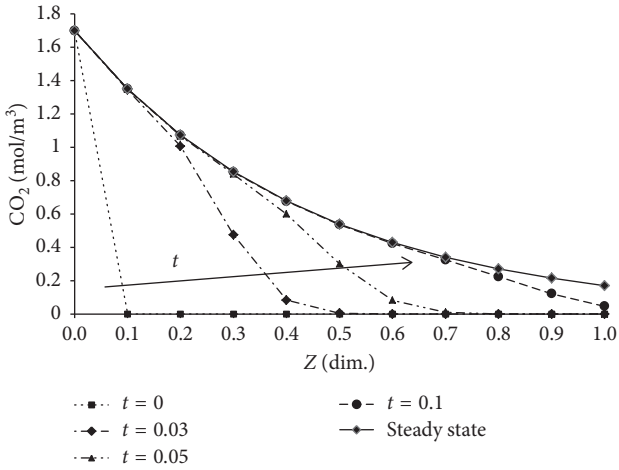

Figure 4: Carbon dioxide axial concentration profiles at different times.

($[RNH_3^+]$) and the carbamate ion ($[RNHCOO^-]$), are produced by this reaction and consumed by reactions (13) and (14), respectively. The interaction between these ions and MEA is very complex and varies with time. In Figures 5 and 6, we show contour plots which describe the variations of the ionic species axial profiles with time. In Figures 5 and 6, the depth axis depicts the axial variation of the concentration from the bottom to the top, i.e., it is a view from the bottom. The horizontal axis shows the time change of the concentration profile. Low values are represented by blue colors, while high values are represented by red colors. The "back" wall represents ionic input values, while the left-side wall represents initial conditions.

The cation profile is shown in Figure 5. The figure shows that the values of the cation concentration are initially very high throughout the column and decrease as time increases. The cation concentration is equal to zero at the column top ($Z = 1$), passes through a maximum, and decreases as it moves to the bottom ($Z = 0$). As time increases, the concentration of the cation decreases at the bottom of the column. Our results show that the decrease in the cation concentration leads to an increase in both the anion concentration and the neutral solvent. This behavior is produced by the complex interaction among the different chemical reactions.

Figure 6 depicts the time evolution of the carbamate ($[RNHCOO^-]$) ion concentration. The anion is not present in the input solution at the top ($Z = 1$); its concentration increases as CO_2 moves upwards in the gas phase, until a maximum is reached at the bottom, coinciding with the highest CO_2 concentration at the bottom of the column ($Z = 0$). The concentration values of the ammonium-like ion were also higher than the carbamate concentration values in all simulations.

The time variation of the solvent MEA concentration is shown in Figure 7.

It is shown in Figure 7 that as the amount of the reaction products increases, we can expect that the amount of the free amine will decrease. An analysis of the three contour plots shows that, at short times, there is a high rate of generation of the cation by consumption of the MEA solvent. As time increases, the concentration of the cation decreases, while the concentration of the anion increases, and some increase of the solvent concentration is observed until equilibrium is achieved.

The main goal of this project is to develop a dynamic simulator for nuclear energy applications. The dynamic simulator is evaluated by how it describes sudden changes in input parameters. In order to test our model, we simulated the response to two sudden changes in input CO_2 concentrations: (i) a step which permanently increases the CO_2 input concentration and (ii) a discrete pulse which increases the input concentration during a fixed time; then, the input concentration is set to its original value (Figures 8 and 9). In the case of a step change in input concentration, we assumed that the column reaches the steady-state operating conditions shown in Figure 4; this is the starting time for the simulation ($t = 0$). At $t = 0$, we double the value of the CO_2 input concentration. The results are shown in Figure 8 where the CO_2 gas-phase concentration starts increasing in value from the bottom of the column (input) towards the top (output) until a new equilibrium is achieved at higher concentration values ($t > 0.1$).

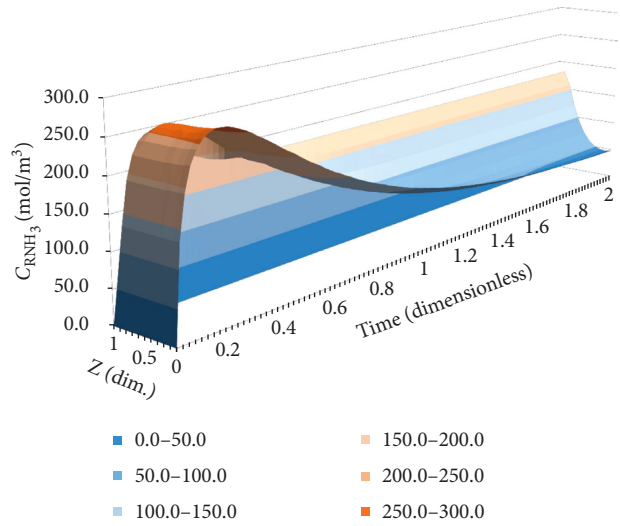

Figure 5: Time variation of the RNH_3^+ concentration profile.

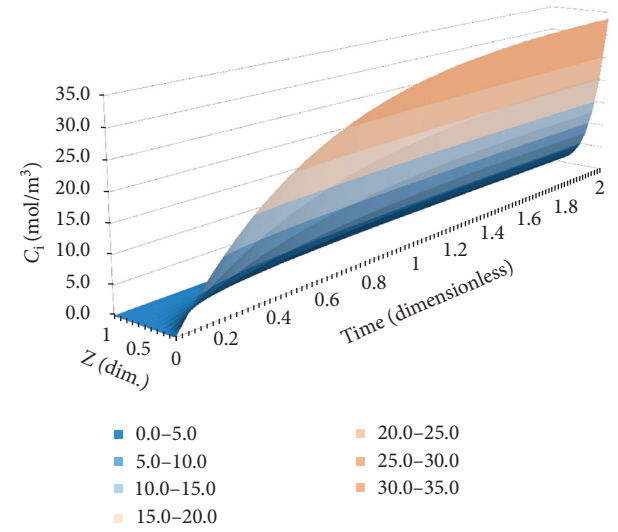

Figure 6: Time variation of the axial concentration profile of the alkanolamine anion.

There is a continuous increase in CO_2 concentration until the new steady-state values are reached. The area between both curves is proportional to the amount of extra mass added.

The simulation results for a discrete pulse are shown in Figure 9. We start from the final equilibrium concentration profile shown in Figure 8 ($t = 0$). At $t = 0$, the CO_2 input concentration is set to its original value (1.7 mol/m^3), and the CO_2 concentration starts decreasing throughout the column. This behavior is more noticeable at the bottom of the column, as the extra amount of CO_2 injected during the pulse travels through the column. The solid line in Figure 9 represents the final steady value to be reached, equal to the one depicted in Figure 4 for the same CO_2 input concentration. At this point in time, all the extra mass injected by the pulse has been absorbed and removed from the gas phase. The area in between the steady-state curve and the CO_2 concentration profile at a particular time represents the remaining extra CO_2 mass injected during the pulse.

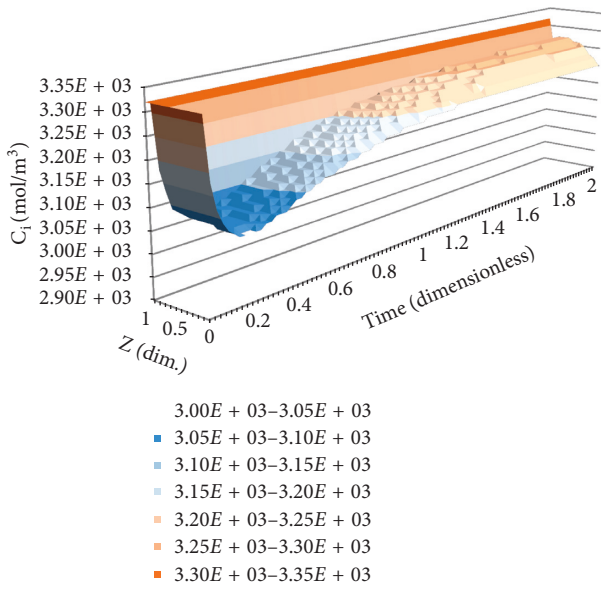

Figure 7: MEA axial concentration profile variation with time.

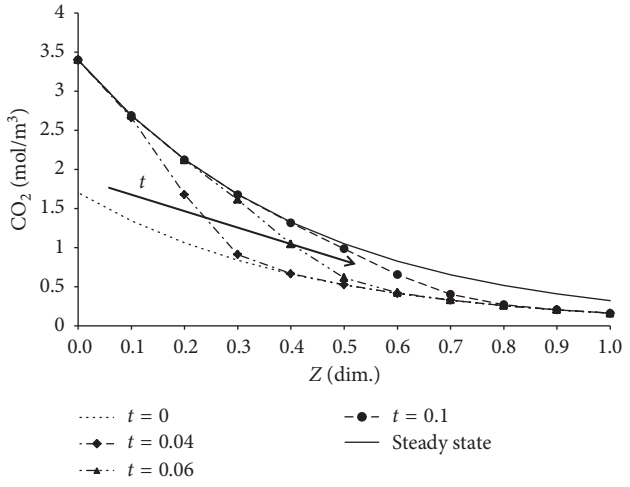

Figure 8: Dynamic change of the CO_2 profile produced by doubling the input CO_2 concentration.

The results presented in Figures 8 and 9 show that the proposed model can be successfully used to analyze the response of the absorption column to sudden changes in CO_2 input concentrations.

3. Conclusions

A model for the dynamic behavior of reactive CO_2 absorption using mixtures of alkanolamine solvents has been successfully developed. The model is based upon transient mass and energy balances for several different chemical species commonly present in CO_2 gas-liquid absorption. The phase equilibrium has been considered using a thermodynamic model and through the use of experimentally based Henry's law values. Typical values for the geometric parameters of the absorber and the packing characteristics have been collected. A reaction scheme that takes into account the different

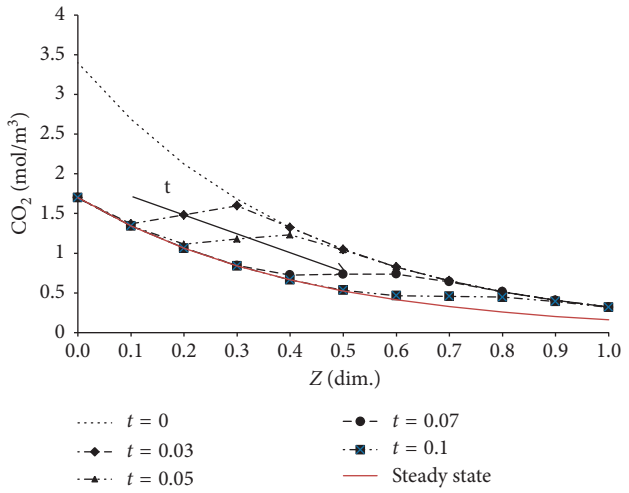

Figure 9: Dynamic change of the CO_2 profile after changing CO_2 input concentration.

reactions between CO_2 and blends of amines in an alkaline environment has been proposed. A computer code has been written to implement the proposed model. The computer code has been validated by checking the values of parameters calculated and comparing results to those reported in the literature. The mass balances for CO_2 have been close within a 0.01% relative error, while the alkanolamine solvents' mass balances have been closed within the computer code precision (10^{-6}). The results have been collected, and they are logical and agree with equivalent literature results. The computer code developed in this work can describe adequately the dynamic processes occurring due to sudden changes in operating conditions. Therefore, it is a valuable tool to design, optimize, and control absorption processes in the nuclear industries.

Appendix

A. Overall CO_2 Mass Transfer Coefficient

The computer code developed to implement our model calculates an overall mass transfer coefficient based upon liquid-phase concentrations ($K^l_{CO_2}$) and compares its value with the liquid-layer mass transfer coefficient ($k^l_{CO_2}$) value to decide which one should be used at each step of the calculations. Typical results are presented in Table 2. Equation (8) was used to calculate $K^l_{CO_2}$. We can see that, in most of the calculations presented in this work, the relative error between using $k^l_{CO_2} E$ and $K^l_{CO_2}$ is around 10%; therefore, the overall mass transfer coefficient is used.

B. Reaction List

The 8 reactions used in the kinetic model are listed below:

$$CO_2 + 2RNH_2 \Longleftrightarrow RNH_3^+ + RNHCOO^- \quad (B.1)$$

$$CO_2 + H_2O \Longleftrightarrow HCO_3^- + H^+ \quad (B.2)$$

$$CO_2 + OH^- \Leftrightarrow HCO_3^- \quad (B.3)$$

$$H_2O \Leftrightarrow OH^- + H^+ \quad (B.4)$$

$$RNH_3^+ \Leftrightarrow H^+ + RNH_2 \quad (B.5)$$

$$RNHCOO^- \Leftrightarrow HCO_3^- + RNH_2 \quad (B.6)$$

$$CO_2 + R_1R_2R_3N + H_2O \Leftrightarrow HCO_3^- + R_1R_2R_3NH^+ \quad (B.7)$$

$$R_1R_2R_3NH^+ \Leftrightarrow R_1R_2R_3N + H^+ \quad (B.8)$$

C. Reaction Rates

The equations used to calculate the forward and reverse reactions are

$$-r_{1f} = k_{1f}[CO_2][RNH_2]^2 \left(\text{mol}\cdot\text{s}^{-1}\cdot\text{m}^{-3}\right), \quad (C.1)$$

$$-r_{2f} = k_{2f}[CO_2]x_{H_2O} \left(\text{mol}\cdot\text{s}^{-1}\cdot\text{m}^{-3}\right), \quad (C.2)$$

$$-r_{3f} = k_{3f}[CO_2][OH^-] \left(\text{mol}\cdot\text{s}^{-1}\cdot\text{m}^{-3}\right), \quad (C.3)$$

$$-r_{4f} = k_{4f} \left(\text{mol}\cdot\text{s}^{-1}\cdot\text{m}^{-3}\right), \quad (C.4)$$

$$-r_{5f} = k_{5f}[RNH_3^+] \left(\text{mol}\cdot\text{s}^{-1}\cdot\text{m}^{-3}\right), \quad (C.5)$$

$$-r_{6f} = k_{6f}[RNHCOO^-] \left(\text{mol}\cdot\text{s}^{-1}\cdot\text{m}^{-3}\right), \quad (C.6)$$

$$-r_{7f} = k_{7f}[CO_2][R_1R_2R_3N]x_{H_2O} \left(\text{mol}\cdot\text{s}^{-1}\cdot\text{m}^{-3}\right), \quad (C.7)$$

$$-r_{8f} = k_{8f}[R_1R_2R_3NH^+] \left(\text{mol}\cdot\text{s}^{-1}\cdot\text{m}^{-3}\right), \quad (C.8)$$

$$-r_{1r} = k_{1r}[RNH_3^+][RNHCOO^-] \left(\text{mol}\cdot\text{s}^{-1}\cdot\text{m}^{-3}\right), \quad (C.9)$$

$$-r_{2r} = k_{2r}[HCO_3^-][H^+] \left(\text{mol}\cdot\text{s}^{-1}\cdot\text{m}^{-3}\right), \quad (C.10)$$

$$-r_{3r} = k_{3r}[HCO_3^-] \left(\text{mol}\cdot\text{s}^{-1}\cdot\text{m}^{-3}\right), \quad (C.11)$$

$$-r_{4r} = k_{4r}[OH^-][H^+] \left(\text{mol}\cdot\text{s}^{-1}\cdot\text{m}^{-3}\right), \quad (C.12)$$

$$-r_{5r} = k_{5r}[H^+][RNH_2] \left(\text{mol}\cdot\text{s}^{-1}\cdot\text{m}^{-3}\right), \quad (C.13)$$

$$-r_{6r} = k_{6r}[HCO_3^-][RNH_2] \left(\text{mol}\cdot\text{s}^{-1}\cdot\text{m}^{-3}\right), \quad (C.14)$$

$$-r_{7r} = k_{7r}[HCO_3^-][R_1R_2R_3NH^+] \left(\text{mol}\cdot\text{s}^{-1}\cdot\text{m}^{-3}\right), \quad (C.15)$$

$$-r_{8r} = k_{8r}[R_1R_2R_3N][H^+] \left(\text{mol}\cdot\text{s}^{-1}\cdot\text{m}^{-3}\right). \quad (C.16)$$

Here, x_{H_2O} is the water molar fraction in the feed solvent phase.

D. Kinetic Data

Table 3 summarizes all the rate equations used in the model. The first number in the first column is the equation number used in Appendix. The second number refers to the original equation number used in the article.

E. Simulation Parameters

In our simulation runs, we used a Montz B 200 metal structured packing [2] as typical packing. Table 4 shows typical geometric parameters and operating variables used in the simulation runs.

F. Generation Terms

Assuming the pseudo-steady state for every chemical species, we can calculate the generation terms that enter into the chemical species mass balances. In order to simplify the calculations, we determined an overall rate per reaction according to

$$R_{ai} = r_{if} - r_{ir}. \quad (F.1)$$

Every generation term ($R_{\text{gen}i}$) is calculated by a molar balance using

$$R_{\text{gen1}} = R_{\text{a1}} - R_{\text{a6}}, \quad (F.2)$$

$$R_{\text{gen2}} = R_{\text{a1}} - R_{\text{a5}}, \quad (F.3)$$

$$R_{\text{gen3}} = R_{\text{a2}} + R_{\text{a3}} + R_{\text{a6}}, \quad (F.4)$$

$$R_{\text{gen4}} = R_{\text{a4}} - R_{\text{a3}}, \quad (F.5)$$

$$R_{\text{gen5}} = R_{\text{a5}} + R_{\text{a6}} - 2R_{\text{a1}}, \quad (F.6)$$

$$\begin{aligned} R_{\text{gen6}} &= R_{\text{a7}} - R_{\text{a4}} - R_{\text{a5}}, \\ R_{\text{gen6}} &= -R_{\text{a1}} - R_{\text{a2}} - R_{\text{a3}} - R_{\text{a5}} - R_{\text{a7}}, \end{aligned} \quad (F.7)$$

$$\begin{aligned} R_{\text{gen7}} &= R_{\text{a2}} + R_{\text{a4}} + R_{\text{a5}}, \\ R_{\text{gen7}} &= R_{\text{a2}} + R_{\text{a4}} + R_{\text{a5}} + R_{\text{a8}}, \end{aligned} \quad (F.8)$$

$$R_{\text{gen8}} = R_{\text{a8}} - R_{\text{a7}}, \quad (F.9)$$

$$R_{\text{gen9}} = R_{\text{a7}} - R_{\text{a8}}. \quad (F.10)$$

Nomenclature

a_T: Mass transfer specific area ($m^2 \cdot m^{-3}$)
a_w: Packing specific area ($m^2 \cdot m^{-3}$)

B_i: Concentration of base i participating in reaction (2) ($mol \cdot m^{-3}$)
C_i^*: Interfacial liquid equilibrium concentration ($mol \cdot m^{-3}$)
C_i^j: Concentration of species i in phase j ($mol \cdot m^{-3}$)
C_{pi}^j: Heat capacities of component i in phase j ($J \cdot mol^{-1} K^{-1}$)
D_i: Diffusivity of component i ($m^2 \cdot s^{-1}$)
E: Enhancement factor (dim.)
E_a: Activation energy ($J \cdot mol^{-1}$)
f_i^j: Fugacities of component i in phase j (dim. or Pa)
H^{cc}: Concentration-based Henry's constant (dim.)
Ha: Hatta number (dim.)
k_{bi}: Specific reaction rate constant of base i ($m^3 \cdot mol^{-1} \cdot s^{-1}$)
k_i: Specific reaction rate constant ($m^3 \cdot mol \cdot s^{-1}$ or s^{-1})
k_i^o: Preexponential factor reaction i ($m^3 \cdot mol \cdot s^{-1}$ or s^{-1})
k_{if}: Forward reaction specific rate constant ($m^3 \cdot mol \cdot s^{-1}$ or s^{-1})
k_{ir}: Reverse reaction specific rate constant ($m^3 \cdot mol \cdot s^{-1}$ or s^{-1})
k_i^j: Phase j mass transfer coefficient of species i (m/s)
K_i: Equilibrium constant reaction i (dim. or mol m^{-3})
K_i^l: Overall liquid mass transfer coefficient of species i (m/s)
$N_{i,diff}$: Flow of component i from the liquid phase into the gas phase (mol m^{-3} s^{-1})
$N_{i,diff}^g$: Flow of component i from the gas phase into the liquid phase ($mol \cdot m^{-3} \cdot s^{-1}$)
$R_{gen,i}$: Species i generated/consumed by chemical reaction ($mol \cdot m^{-3} \cdot s^{-1}$)
r_i: Reaction rate for species i ($mol \cdot m^{-3} \cdot s^{-1}$)
R: Gas constant ($J \cdot mol^{-1} \cdot K^{-1}$)
t: Time (s)
T_i: Temperature of the i phase (K)
u_i: Superficial velocity of the i phase ($m \cdot s^{-1}$)
U_T: Global heat transfer coefficient ($J \cdot m^{-2} \cdot K^{-1} \cdot s^{-1}$)
z: Column height (dim.)
Z_g: Compressibility factor (dim.)
ΔH_R: Heat released by chemical reaction ($J \cdot mol^{-1}$)
φ_i^j: Fugacity coefficients for component i in phase j (dim.)
Dim.: Dimensionless.

Data Availability

The data collected during the submitted research project are stored in the authors' servers. The data and metadata collected are stored in Excel spreadsheets and comprise less than 1 GB. They can be made public as required.

Conflicts of Interest

The authors declare that they have no conflicts of interest.

Acknowledgments

Funding for this research provided by the Office of Nuclear Energy of the U.S. Department of Energy, under the Nuclear Energy University Program (Grant # NFE-12-03822), is gratefully acknowledged by the authors. This study was conducted at Prairie View A&M University in collaboration with the Oak Ridge National Laboratory (ORNL). ORNL is managed by UT-Battelle, LLC, under Contract DE-AC05-00OR22725 with the U.S. Department of Energy.

References

[1] A. Ladshaw, S. Yiacoumi, R. Lin, Y. Nan, L. L. Tavlarides, and C. Tsouris, "A mechanistic modeling framework for gas phase adsorption kinetics and fixed-bed transport," *AIChE Journal*, vol. 63, no. 11, pp. 5029–5043, 2017.

[2] T. Greer, "Modeling and simulation of post combustion CO_2 capturing," M.Sc. thesis, Telemark University College, Faculty of Technology, Porsgrunn, Norway, 2008.

[3] A. L. Kohl and R. B. Nielsen, *Gas Purification*, Gulf Publishing, Houston, TX, USA, 5th edition, 1997.

[4] G. F. Versteeg and W. P. M. van Swaaij, "Solubility and diffusivity of acid gases (CO_2, N_2O) in aqueous alkanolamine solutions," *Journal of Chemical & Engineering Data*, vol. 33, pp. 29–34, 1988.

[5] D. P. Hagewiesche, S. S. Ashour, H. A. Al-Ghawas, and O. C. Sandall, "Absorption of carbon dioxide into aqueous blends of monoethanolamine and methyldiethanolamine," *Chemical Engineering Science*, vol. 50, no. 7, pp. 1071–1079, 1995.

[6] H. Bosch, G. F. Versteeg, and W. P. M. van Swaaij, "Gas-liquid mass transfer with parallel reversible reactions-III. Absorption of CO_2 into solutions of blends of amines," *Chemical Engineering Science*, vol. 44, no. 11, pp. 2745–2750, 1989.

[7] R. Sakwattanapong, A. Aroonwilas, and A. Veawab, "Reaction rate of CO_2 in aqueous MEA-AMP solution: experiment and modeling," *Energia Procedia*, vol. 1, no. 1, pp. 217–224, 2009.

[8] P. Usubharatana and P. Tontiwachwuthikul, "Enhancement factor and kinetics of CO_2 capture by MEA-methanol hybrid solvents," *Energia Procedia*, vol. 1, no. 1, pp. 95–102, 2009.

[9] T. Greer, A. Bedelbayev, J. M. Igreja, J. F. Pereira Gomes, and B. Lie, "A dynamic model for the de-absorption of carbon dioxide from monoethanolamine solution," in *Proceedings of SIMS*, Amsterdam, Netherlands, October 2008.

[10] M. Caplow, "Kinetics of carbamate formation and breakdown," *Journal of the American Chemical Society*, vol. 90, no. 24, pp. 6795–6803, 1968.

[11] P. V. Danckwerts, "The reactions of CO_2 with ethanolamines," *Chemical Engineering Science*, vol. 34, no. 4, pp. 443–446, 1979.

[12] G. F. Versteeg and W. P. M. van Swaaij, "On the kinetics between CO_2 and alkanolamines both in aqueous and non-aqueous solutions-I. Primary and secondary amines," *Chemical Engineering Science*, vol. 43, no. 3, pp. 573–585, 1988.

[13] R. J. Littel, W. P. M. van Swaaij, and G. F. Versteeg, "Kinetics of CO_2 with primary and secondary amines in aqueous solution-I. Zwitterion formation deprotonation kinetics for DEA and DIPA in aqueous blends of alkanolamines," *Chemical Engineering Science*, vol. 47, no. 8, pp. 2027–2035, 1992.

[14] C. Alvarez-Fuster, N. Midoux, A. Laurent, and J. C. Charpentier, "Chemical kinetics of the reaction of carbon dioxide with amines in pseudo m-n^{th} order conditions in aqueous and organic solutions," *Chemical Engineering Science*, vol. 35, no. 8, pp. 1717–1723, 1980.

[15] E. Sada, H. Kumazawa, Y. Osawa, M. Matsuura, and Z. Q. Han, "Reaction kinetics of carbon dioxide with amines in non-aqueous solvents," *Chemical Engineering Journal*, vol. 33, no. 2, pp. 87–95, 1986.

[16] R. J. Littel, W. P. M. van Swaaij, and G. F. Versteeg, "Kinetics of carbon dioxide with tertiary amines in aqueous solution," *AIChE Journal*, vol. 36, no. 11, pp. 1633–1640, 1990.

[17] T. L. Donaldson and Y. N. Nguyen, "Carbon dioxide reaction and transportation in aqueous amine membranes," *Industrial & Engineering Chemistry Fundamentals*, vol. 19, no. 3, pp. 260–266, 1980.

[18] G. F. Versteeg and W. P. M. van Swaaij, "On the kinetics between CO_2 and alkanolamines both in aqueous and non-aqueous solutions-II. Ternary amines," *Chemical Engineering Science*, vol. 43, no. 3, p. 587, 1988.

[19] H. Bosch, G. F. Versteeg, and W. P. M. van Swaaij, "Gas-liquid mass transfer with parallel reversible reactions-I. Absorption of CO_2 into solutions of sterically hindered amines," *Chemical Engineering Science*, vol. 44, no. 11, pp. 2723–2734, 1989.

[20] B. P. Mandal, M. Guhab, A. K. Biswasb, and S. S. Bandyopadhyaya, "Removal of carbon dioxide by absorption in mixed amines: modelling of absorption in aqueous MDEA-MEA and AMP-MEA solutions," *Chemical Engineering Science*, vol. 56, no. 21-22, pp. 6217–6224, 2001.

[21] A. Benamor and M. K. Aroua, "Modeling of CO_2 solubility and carbamate concentration in DEA, MDEA and their mixtures using the Deshmukh-Mather model," *Fluid Phase Equilibria*, vol. 231, no. 2, pp. 150–162, 2005.

[22] A. Jamal, A. Meisen, and C. Jim Lim, "Kinetics of carbon dioxide absorption and desorption in aqueous alkanolamine solutions using a novel hemispherical contactor—II: experimental results and parameter estimation," *Chemical Engineering Science*, vol. 61, no. 19, pp. 6590–6603, 2006.

[23] S. Freguia and G. T. Rochelle, "Modeling of CO_2 capture by aqueous monoethanolamine," *AIChE Journal*, vol. 49, no. 7, pp. 1676–1686, 2003.

[24] A. Bedelbayev, T. Greer, and B. Lie, "Model based control of absorption tower for carbon dioxide capturing," in *Proceedings of SIMS*, pp. 1420–1440, Amsterdam, Netherlands, February 2008.

[25] N. Haimour, A. Bidarian, and O. Sandall, "Kinetics of the reaction between carbon dioxide and methyldiethanolamine," *Chemical Engineering Science*, vol. 42, no. 6, pp. 1393–1398, 1987.

[26] J. E. Critchfield, "CO_2 absorption/desorption in methyldiethanolamine solutions promoted with MEA and D2EA. Mass transfer and reaction kinetics," Ph. D. thesis, University of Texas, Austin, TX, USA, 1988.

[27] H. A. Rangwala, B. R. Morrell, A. E. Mather, and F. D. Otto, "Absorption of CO_2 into aqueous tertiary amine/MEA solutions," in *Proceedings of AIChE National Meeting*, vol. 8, New Orleans, LA, USA, March 1988.

[28] B. R. W. Pinsent, L. Pearson, and F. J. W. Roughton, "The kinetics of combination of carbon dioxide with hydroxide ions," *Journal of the Chemical Society, Faraday Transactions*, vol. 52, pp. 1512–1520, 1956.

[29] Y. Liu, L. Zhang, and S. Watanasiri, "Representing vapour-liquid equilibrium for an aqueous MEA-CO_2 system using the electrolyte non-random-two-liquid model," *Industrial & Engineering Chemistry Research*, vol. 38, no. 5, pp. 2080–2090, 1999.

[30] L. L. Tavlarides, R. Lin, Y. Nan et al., *Sorption Modeling and Verification for Off-Gas Treatment*, NEUP, Washington, DC, USA, 2015, https://neup.inl.gov/.

[31] R. H. Perry and D. W. Green, *Chemical Engineers Handbook*, McGraw-Hill, New York, NY, USA, 7th edition, 1999.

[32] G. F. Versteeg, J. V. Holst, P. P. Politiek, and J. P. Niederer, "CO_2 capture from flue gas using amino acid salt solutions," June 2006, http://www.co2-cato.nl/doc.php?lid=317.

[33] C. Gòmez, D. O. Borio, and N. S. Schbib, "Simulation of an industrial packed column for reactive absorption of CO_2," *Latin American Applied Research*, vol. 33, pp. 201–205, 2003.

[34] E. P. Van Elk, M. C. Knaap, and G. F. Versteeg, "Application of the penetration theory for gas-liquid mass transfer without liquid bulk differences with systems with a bulk," *IChemE Symposium Series*, vol. 152, 2006.

[35] J. Gabitto and C. Tsouris, "Dynamic simulation of CO_2 absorption in a packing tower," in *Proceedings of AIChE Annual Meeting*, vol. 11, Atlanta, GA, USA, November 2014.

[36] A. Lawal, M. Wang, P. Stephenson, and H. Yeubg, "Dynamic modeling of CO_2-absorption for post combustion capture in coal-fired power plants," *Fuel*, vol. 88, no. 12, pp. 2455–2462, 2009.

[37] J. H. Richardson, J. H. Harker, and J. R. Backhurst, *Chemical Engineering*, vol. 2, Particle Technology and Separation Processes, Butterworth-Heinemann, Publishers, Oxford, UK, 5th edition, 2008.

[38] R. Billet and M. Schultes, "Prediction of mass transfer columns with dumped and arranged packing's: updated summary of the calculation method of billet and schultes," *Chemical Engineering Research and Design*, vol. 77, no. 6, pp. 498–504, 1999.

[39] A. Aboudheir, P. Tontiwachwuthikula, A. Chakmab, and R. Idema, "Kinetics of the reactive absorption of carbon dioxide in high CO_2-loaded, concentrated aqueous monoethanolamine solutions," *Chemical Engineering Science*, vol. 58, no. 23-24, pp. 5195–5210, 2003.